CrystEngComm

PAPER

View Article Online
View Journal | View Issue

Check for updates

Cite this: *CrystEngComm*, 2018, **20**, 7458

Optimizing the oxygen balance by changing the A-site cations in molecular perovskite high-energetic materials†

Shao-Li Chen, ‡ Yu Shang, ‡ Chun-Ting He, Lin-Ying Sun, Zi-Ming Ye, Wei-Xiong Zhang * and Xiao-Ming Chen *

We presented two new members of molecular perovskite high-energetic materials, $(H_2pz)[Na(ClO_4)_3]$ (PAP-1) and $(H_2dabco\text{-}O)[K(ClO_4)_3]$ (DAP-O2), in which H_2pz^{2+} (piperazine-1,4-diium) and $H_2dabco\text{-}O^{2+}$ (1-hydroxy-1,4-diazabicyclo[2.2.2]octane-1,4-diium) act as A-site fuel cations, respectively. Compared with their H_2dabco^{2+} analogues, $(H_2dabco)[M(ClO_4)_3]$ (H_2dabco^{2+} = 1,4-diazabicyclo[2.2.2]octane-1,4-diium, M = Na^+ for DAP-1 and K^+ for DAP-2, respectively), PAP-1 and DAP-O2 exhibit optimized oxygen balance by employing two strategies to change the A-site cations, *i.e.*, "trimming the C and H atoms" of H_2dabco^{2+} by using H_2pz^{2+} to form PAP-1 and adding an O atom into H_2dabco^{2+} by using $H_2dabco\text{-}O^{2+}$ to form DAP-O2, respectively. As suggested by DFT calculations and the K–J equation, the smaller H_2pz^{2+} cation in PAP-1 gives a significantly-optimized oxygen balance from −22.0% to −3.9% and an increased crystal density from 2.02 to 2.07 g cm^{-3}, resulting in a better detonation performance for PAP-1. Meanwhile the larger $H_2dabco\text{-}O^{2+}$ cation gives a slightly-optimized oxygen balance from −21.3% to −17.1% but a decreased crystal density from 2.04 to 1.98 g cm^{-3}, leading to a decreased detonation performance from DAP-2 to DAP-O2. This study demonstrated how to rationally choose the A-site cations in a perovskite structure for modulating the properties of molecular perovskite high-energetic materials, providing important clues for designing more advanced energetic materials for practical use.

Received 11th August 2018,
Accepted 12th October 2018

DOI: 10.1039/c8ce01350k

rsc.li/crystengcomm

Introduction

Since black powder was invented by ancient Chinese, energetic materials, as one of the most influential materials in human history, have been widely investigated.[1–3] Promoted by the joint efforts of synthetic and theoretical investigations, the past few decades have witnessed a rapid development of high-energetic materials,[4] especially nitrogen-rich organic energetic molecules,[5–17] as well as their ionic salts,[18–23] coordination polymers[24–30] and metal–organic frameworks.[31–40] However, for most single explosives, the increase in detonation performance generally causes instability, sensitivity and high cost. Such a contradiction between the denotation performance, stability, and cost results in a frustrating fact that the currently best practicable single explosive is still HMX (cyclotetramethylene tetranitramine), invented during the Second World War, despite its average performance and high cost.[4] Therefore, seeking an ideal balance between the denotation performance, stability, and cost is a long-term challenge for the evolution of practicable single explosives.

To design energetic compounds *via* simple synthetic routes, with low production costs and easy scale-up, we proposed a new strategy that assembles the low-cost molecular oxidizer and fuel components into ternary crystals with a specified structure. Different from the traditional design focusing on the modification of intra-molecular functional groups, our strategy emphasises the inter-molecular self-assembly that could be easily achieved in solution under ambient conditions by judiciously choosing the molecular components. Compared with the early-explored simple energetic binary salts, ternary crystals provide much room for material design as well as performance modulation.[41,42] As the simplest high-symmetry structure for ternary crystals, the perovskite structure is very attractive, and perovskite materials always stand at the forefront of materials science.[43–50] In our previous work,[51–53] we employed the perovskite structure to incorporate oxidative ClO_4^- anions and reductive H_2dabco^{2+} cations (1,4-diazabicyclo[2.2.2]octane-1,4-diium) into ternary crystals with the aid of different alkali/ammonium cations, and obtained four molecular perovskite high-energetic

---

*MOE Key Laboratory of Bioinorganic and Synthetic Chemistry, School of Chemistry, Sun Yat-Sen University, Guangzhou 510275, China.
E-mail: zhangwx6@mail.sysu.edu.cn, cxm@mail.sysu.edu.cn*

† Electronic supplementary information (ESI) available. CCDC 1860906, 1860907, 1872452 and 1872410. For ESI and crystallographic data in CIF or other electronic format see DOI: 10.1039/c8ce01350k

‡ These authors contributed equally to this work.

materials, $(H_2dabco)[M(ClO_4)_3]$ ($M = Na^+$, K^+, Rb^+, and NH_4^+ for DAP-1, -2, -3, and -4, respectively). The previous study revealed that the alternately dense packing of oxidative ClO_4^- anions and reductive organic cations in the perovskite structure gives rise to a new class of advanced single explosives possessing a detonation performance superior to HMX, a higher stability than HMX, and importantly, a much lower cost than HMX.

Moreover, by taking advantage of the tuneable/modifiable characteristics of the A, B and X components, such molecular perovskites provide an opportunity to tailor the performances of high-energetic materials. In principle, diverse molecular components with suitable valence, shape and size can be assembled into such kinds of ternary crystals to modulate the properties such as oxygen balance, crystal density, and stability as well as detonation performance. To investigate the capacity of molecular perovskites to optimize the oxygen balance by the A-site fuel cations, as a continued work, we herein presented two new members of molecular perovskite high-energetic materials, $(H_2pz)[Na(ClO_4)_3]$ (PAP-1) and $(H_2dabco\text{-}O)[K(ClO_4)_3]$ (DAP-O2), in which H_2pz^{2+} (piperazine-1,4-diium) and $H_2dabco\text{-}O^{2+}$ (1-hydroxy-1,4-diazabicyclo[2.2.2]-octane-1,4-diium) act as A-site fuel cations, respectively. As shown in Scheme 1, compared with the previously-used H_2dabco^{2+} cation, these two A-site fuel cations presented two strategies for optimizing oxygen balances, *i.e.*, "trimming the C and H atoms" of H_2dabco^{2+} by using H_2pz^{2+} to generate PAP-1 and adding an O atom into H_2dabco^{2+} by using $H_2dabco\text{-}O^{2+}$ to give DAP-O2, respectively. The influences on the detonation performances and stabilities of these two strategies are discussed, based on the combined techniques of single-crystal/powder X-ray diffraction and thermal analyses, as well as theoretical evaluations of the detonation parameters.

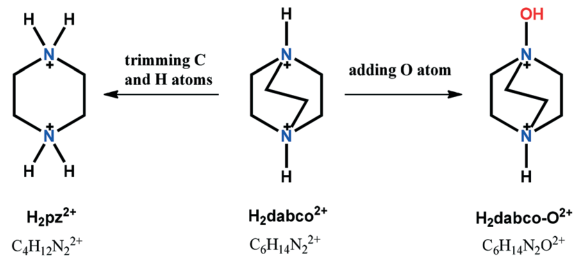

Scheme 1 Two strategies for optimizing oxygen balance.

Experimental section

Materials and methods

All chemicals were obtained from commercial sources and used without further purification. DSC measurements were performed by heating and cooling the powder sample on a TA Q2000 instrument. The PXRD patterns (Cu-Kα) for identifying the phase purity were collected on a Bruker Advance D8 diffractometer using the Bragg–Brentano geometry. The enthalpy of formation was approximated by obtaining the constant volume combustion energies ($\Delta_c U$) using a big oxygen bomb calorimeter (No. 24391170) with a volume of about 5.0 L and a calorie limit of 203 kJ made by the Xi'an Modern Chemistry Research Institute (Xi'an, China). The detonation parameters were calculated using the EXPLO5 v6.04.02 computer code. The impact sensitivity was tested on a BFH 10 BAM impact apparatus. The friction sensitivity was tested on a FSKM 10 BAM friction apparatus.

Synthesis of $(H_2pz)[Na(ClO_4)_3]$ (PAP-1)

Different from the previously-reported method that directly dissolves piperazine, $NaClO_4$, and $HClO_4$ with a molar ratio of 1 : 1 : 2 in distilled water,[43] in this work, sodium perchlorate (1 mmol) was added into an aqueous solution (5 mL) of piperazine (1 mmol), then a 70% perchloric acid solution was added into the solution. The colourless products were obtained by filtration and washed three times with ethanol, in a yield of 80% based on $NaClO_4$.

Synthesis of $(H_2dabco\text{-}O)[K(ClO_4)_3]$ (DAP-O2)

Triethylenediamine (1 mmol) was dissolved in 30% hydrogen peroxide (molar ratio 1 : 3) and stirred at 0 °C for 5 min, then concentrated and filtered to gain dabco-O solid products. Potassium perchlorate (1 mmol) was added into an aqueous solution (20 mL) of dabco-O (1 mmol), then mixed with a 70% perchloric acid solution. The colourless products were also obtained by filtration and washed three times with ethanol, in a yield of 60% based on $KClO_4$.

Caution: Although they were safe to use during the syntheses in the course of this research, these energetic materials need to be handled with extreme care. The mixtures of perchloric acid and organic liquids are highly sensitive, so do not mix them without the corresponding perchlorate salt.

X-ray crystallography

The colourless block single crystals of PAP-1 and DAP-O2 for X-ray diffraction were obtained by evaporating the filtrates after several days. The diffraction intensities of PAP-1 and DAP-O2 at 223 K were collected on a SuperNova AtlasS2 diffractometer with graphite-monochromated Mo-Kα radiation (λ = 0.71073 Å). The diffraction intensities of PAP-1 and DAP-O2 at room temperature were collected on a Rigaku XtaLAB P300DS diffractometer with graphite-monochromated Cu-Kα radiation (λ = 1.54184 Å) and Mo-Kα radiation (λ = 0.71073 Å), respectively. The structures were solved with the SHELXS structure solution program using direct methods and refined with the SHELXL refinement package using a full-matrix least-squares technique. Anisotropic displacement parameters were applied to all non-hydrogen atoms except for the highly-disordered $H_2dabco\text{-}O^{2+}$ cation. All the hydrogen atoms were generated geometrically. Crystallographic data are summarized in Table 1. The CIFs were deposited in the

Table 1 Thermal data from DSC measurements

Compounds	T_d[a]/°C	T_p[b]/°C	Q_{DSC}[c]/kJ g^{-1}	Ref.
DAP-1	344	361	4.40	52
PAP-1	371	375	4.69	This work
DAP-2	364	377	4.08	52
DAP-O2	329	360	4.53	This work

[a] The onset decomposition temperatures. [b] The peak decomposition temperatures. [c] The heat of decomposition recorded by DSC.

Cambridge Crystallographic Data Centre, CCDC numbers: 1860906, 1860907, 1872452 and 1872410, respectively.

Results and discussion

Single-crystal structures

Single-crystal X-ray crystallography showed that PAP-1 crystallizes in the monoclinic space group $P2_1/c$[43] at both 293 K and 223 K, while DAP-O2 crystallizes in the cubic space group $Fm\bar{3}c$ at 293 K and $P2_1/c$ at 223 K. The structures of both PAP-1 and DAP-O2 are of perovskite type, by regarding H_2pz^{2+} or $H_2dabco\text{-}O^{2+}$ as the A-site cation, Na^+ or K^+ as the B-site cation, and ClO_4^- as the X-bridges. That is, in PAP-1 (or DAP-O2), each Na^+ (or K^+) ion is surrounded by twelve oxygen atoms from six ClO_4^- anions, while each ClO_4^- anion bridges two Na^+ (or K^+) ions, forming a three-dimensional anionic framework consisting of cages that are filled with H_2pz^{2+} (or $H_2dabco\text{-}O^{2+}$) cations.

Compared with H_2dabco^{2+} in DAP-1, the H_2pz^{2+} cation is smaller and possesses a lower symmetry; accordingly, the anionic framework constructed from Na^+ and ClO_4^- is distorted in PAP-1, as indicated by the fact that PAP-1 crystallizes in a monoclinic space group rather than a cubic one. As such a distorted framework could accumulate the H_2pz^{2+} cations in a more compact way, PAP-1 has a slightly-higher crystal density (2.07 g cm^{-3}) than DAP-1 (2.02 g cm^{-3}) at room temperature. Accordingly, the average Na⋯Cl atomic distance in PAP-1 (3.453 Å, see Table S2†) is shorter than that in DAP-1 (3.551 Å). These facts indicated that, owing to the smaller A-site cation, the anionic framework in PAP-1 has a weaker structural tension than that in DAP-1.

At 223 K, similar to PAP-1, DAP-O2 crystallizes in the monoclinic phase because the $H_2dabco\text{-}O^{2+}$ cation also possesses a lower symmetry than the H_2dabco^{2+} cation. However, the order–disorder transition of such larger $H_2dabco\text{-}O^{2+}$ cations allows DAP-O2 to undergo multi-step phase transitions (Fig. S6†), and be in a cubic phase ($Fm\bar{3}c$) at room temperature (Fig. 1b). Compared with its H_2dabco^{2+} analogue (DAP-2), DAP-O2 has a slightly-larger anionic framework (constructed from K^+ and ClO_4^-) that is propped up by larger cations, as suggested by the fact that the average K⋯Cl atomic distance in DAP-O2 (3.670 Å, see Table S2†) is longer than that in DAP-2 (3.578 Å) at 223 K. Accordingly, the larger unit-cell volume of DAP-O2 results in a decrease of crystal density (1.98 g cm^{-3}) compared with that of DAP-2 (2.04 g cm^{-3}) at room temperature. These facts suggested that DAP-O2 has a stronger structural tension than DAP-2 because of the steric requirement of the larger $H_2dabco\text{-}O^{2+}$ cation. It is worth mentioning that we have also tried to assemble smaller H_2pz^{2+} cations into the larger $[K(ClO_4)_3]^{2-}$ framework and to assemble the larger $H_2dabco\text{-}O^{2+}$ cations into the smaller $[Na(ClO_4)_3]^{2-}$ framework, but all the attempts failed, implying the importance of size matching in choosing the molecular components for constructing molecular perovskites.

Thermal stability

The onset decomposition temperature (T_d) measured by DSC was 371 °C for PAP-1 and 329 °C for DAP-O2 (Table 1), respectively. Compared with the corresponding analogues, PAP-1 has a higher thermal stability than DAP-1 (344 °C), whereas DAP-O2 has a lower thermal stability than DAP-2 (364 °C). Such contrasting behaviours of PAP-1 and DAP-O2 may be ascribed to the difference in their structural tensions, namely,

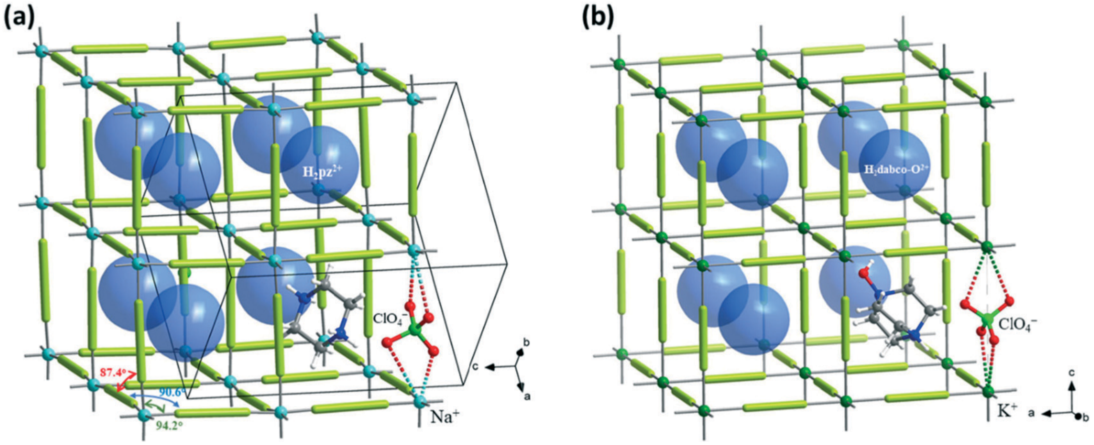

Fig. 1 The structures of PAP-1 in the monoclinic space group $P2_1/c$ at 223 K (a) and DAP-O2 in the cubic space group $Fm\bar{3}c$ at 293 K (b). For clarity, only one A-site cation and X-site chlorate anion are shown but other A-site cations and X-site anions are presented as light-blue spheres and yellow-green cylinders, respectively.

a weaker structural tension could improve the thermal stability, while a stronger one could reduce the thermal stability. It is worth noting that the T_ds of these molecular perovskite energetic materials are higher than those of classical single explosives, such as TXT, RDX, HMX and CL-20, thanks to the stable covalent-bonds of the molecular components and the inter-ionic Coulomb interactions.

Detonation parameters

In our previous work,[52] oxygen-bomb calorimetry was employed to measure the heat of formation that was further inputted into EXPLO5 to predict the detonation performance. As the oxygen-bomb calorimetry measurements usually overestimate the heat of formation for halogen containing compounds (see the ESI†), herein, we adopted density functional theory (DFT) and the K–J equation (see the ESI†) to evaluate the detonation parameters for the DAPs. As listed in Table 2 and Fig. 2, the DFT calculation suggested that both DAP-1 and PAP-1 have better detonation performances than RDX, while DAP-2 and DAP-O2 have similar detonation performances to RDX. Compared with its H_2dabco^{2+} analogue (DAP-1), PAP-1 has a reduced heat of detonation (6.39 → 5.77 kJ g^{-1}), but increased detonation velocity (8.781 → 8.917 km s^{-1}) and detonation pressure (36.5 → 38.2 GPa). Such an increase in the performance of PAP-1 should be attributed to the improvement on both oxygen balance (−22.0% and −3.9% for DAP-1 and PAP-1, respectively) and crystal density (2.02 and 2.07 g cm^{-3} for DAP-1 and PAP-1, respectively). In contrast, when DAP-O2 was compared with its H_2dabco^{2+} analogue (DAP-2), the performances are slightly decreased: heat of detonation (6.12 → 5.69 kJ g^{-1}), detonation velocity (8.591 → 8.327 km s^{-1}) and detonation pressure (35.2 → 32.5 GPa), which should be ascribed to the fact that adding an O atom into H_2dabco^{2+} by using $H_2dabco\text{-}O^{2+}$ cations only gives a slightly-optimized oxygen balance from −21.3% to −17.1% but causes a decrease in crystal density from 2.04 to 1.98 g cm^{-3}. Nevertheless, it should be pointed out that the real detonation reactions are very complicated; therefore, the aforementioned calculations could only roughly estimate the detonation performances as they are based on the assumed detonation reaction and empirical K–J equation with low precision. It is necessary to accurately measure the detonation parameters by performing experiments on the molecular perovskite materials in the next stage.

Table 2 Detonation properties of some well-known explosives and the series of molecular perovskite high-energetic materials

Compound	ρ^a (g cm^{-3})	Q^b (kJ g^{-1})	D^b (km s^{-1})	P^b (GPa)	OB^c (%)
TNT	1.65	3.74	6.897	20.0	−74.0
RDX	1.82	5.59	8.634	33.3	−21.6
HMX	1.96	5.58	9.096	38.6	−21.6
DAP-1	2.02[a]	6.39	8.781	36.5	−22.0
PAP-1	2.07[a]	5.77	8.917	38.2	−3.9
DAP-2	2.04[a]	6.12	8.591	35.2	−21.3
DAP-O2	1.98[a]	5.69	8.327	32.5	−17.1

[a] ρ is the density of the powder sample measured by capillary powder X-ray diffraction at room temperature; for classic explosives, ρ is the crystal density. [b] Q is the heat of detonation, D is the detonation velocity, and P is the detonation pressure. The detonation parameters were estimated by DFT calculations and the empirical K–J equation. [c] Oxygen balances based on CO_2 for $C_aH_bN_cM_dCl_eO_f$, where M is the alkali metal ion, were calculated by: $OB[\%] = 1600[f - 2a - (b - e + d)/2]/M_W$, where M_W is the molecular weight.

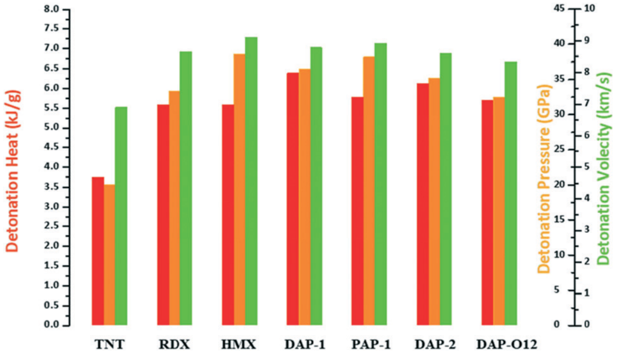

Fig. 2 Bar chart representation of detonation parameters evaluated by DFT calculations and the K–J equation, for DAP-1, DAP-2, PAP-1, DAP-O2, and well-known classical organic explosives including TNT, RDX and HMX.

Conclusions

In summary, we presented two new members of molecular perovskite high-energetic materials, *i.e.*, PAP-1 and DAP-O2, whose oxygen balances are optimized and compared with their H_2dabco^{2+} analogues, *i.e.*, DAP-1 and DAP-2, respectively, by employing two strategies for changing the A-site fuel cation, *i.e.*, trimming the C and H atoms of the H_2pz^{2+} cation in PAP-1 and adding an O atom to the $H_2dabco\text{-}O^{2+}$ cation in DAP-O2, respectively. Such two strategies have different influences on the overall performances. Trimming the C and H atoms from H_2dabco^{2+} to afford a smaller H_2pz^{2+} cation gives a significantly-optimized oxygen balance from −22.0% to −3.9% and an increased crystal density from 2.02 to 2.07 g cm^{-3}, resulting in improved detonation performances from DAP-1 to PAP-1. In contrast, adding an O atom to H_2dabco^{2+} to afford a larger $H_2dabco\text{-}O^{2+}$ cation only gives a slightly-optimized oxygen balance from −21.3% to −17.1% but causes a decrease in crystal density from 2.04 to 1.98 g cm^{-3}, resulting in a decreased detonation performance from DAP-2 to DAP-O2. The present work demonstrated how to rationally choose the A-site cations in the perovskite structure to modulate the properties of molecular perovskite high-energetic materials, providing important clues for designing more advanced energetic materials for practical use.

Conflicts of interest

There are no conflicts to declare.

Acknowledgements

This work was supported by the NSFC (21290173 and 21722107). The authors thank the Xi'an Modern Chemistry Research Institute (Xi'an, China) for preforming the oxygen-bomb calorimetry.

Notes and references

1 R. Meyer, J. Köhler and D. I. A. Homburg, *Explosives*, Wiley, Sixth edn, 2007.

2 T. Brinck, *Green Energetic Materials*, Wiley, 2014.

3 J. A. Conkling and C. J. Mocella, *Chemistry of Pyrotechnics*, CRC Press, 2010.

4 J. P. Agrawal, *High Energy Materials: Propellants, Explosives and Pyrotechnics*, 2010.

5 N. Fischer, D. Fischer, T. Klapotke, D. Piercey and J. Stierstorfer, *J. Mater. Chem.*, 2012, **22**, 20418–20422.

6 Z. Xu, G. Cheng, H. Yang, X. Ju, P. Yin, J. Zhang and J. M. Shreeve, *Angew. Chem., Int. Ed.*, 2017, **56**, 5877–5881.

7 D. Kumar, G. H. Imler, D. A. Parrish and J. M. Shreeve, *J. Mater. Chem. A*, 2017, **5**, 16767–16775.

8 T. T. Vo, J. Zhang, D. A. Parrish, B. Twamley and J. M. Shreeve, *J. Am. Chem. Soc.*, 2013, **135**, 11787–11790.

9 Y. Wang, Y. Liu, S. Song, Z. Yang, X. Qi, K. Wang, Y. Liu, Q. Zhang and Y. Tian, *Nat. Commun.*, 2018, **9**, 2444.

10 Q. Yu, P. Yin, J. Zhang, C. He, G. H. Imler, D. A. Parrish and J. M. Shreeve, *J. Am. Chem. Soc.*, 2017, **139**, 8816–8819.

11 G. Bélanger-Chabot, M. Rahm, R. Haiges and K. O. Christe, *Angew. Chem.*, 2015, **127**, 11896–11900.

12 C. B. Aakeroy, T. K. Wijethunga and J. Desper, *Chem. – Eur. J.*, 2015, **21**, 11029–11037.

13 K. B. Landenberger and A. J. Matzger, *Cryst. Growth Des.*, 2012, **12**, 3603–3609.

14 C. Guo, H. Zhang, X. Wang, J. Xu, Y. Liu, X. Liu, H. Huang and J. Sun, *J. Mol. Struct.*, 2013, **1048**, 267–273.

15 K. B. Landenberger, O. Bolton and A. J. Matzger, *J. Am. Chem. Soc.*, 2015, **137**, 5074–5079.

16 J. C. Bennion, Z. R. Siddiqi and A. J. Matzger, *Chem. Commun.*, 2017, **53**, 6065–6068.

17 T. S. Hermann, K. Karaghiosoff, T. M. Klapotke and J. Stierstorfer, *Chem. – Eur. J.*, 2017, **23**, 12087–12091.

18 J. Zhang, S. Dharavath, L. A. Mitchell, D. A. Parrish and J. M. Shreeve, *J. Am. Chem. Soc.*, 2016, **138**, 7500–7503.

19 J. Zhang, Q. Zhang, T. T. Vo, D. A. Parrish and J. M. Shreeve, *J. Am. Chem. Soc.*, 2015, **137**, 1697–1704.

20 X. Li, X. Liu, S. Zhang, H. Wu, B. Wang, Q. Yang, Q. Wei, G. Xie, S. Chen and S. Gao, *J. Chem. Eng. Data*, 2015, **61**, 207–212.

21 W. Liu, W. L. Liu and S. P. Pang, *RSC Adv.*, 2017, **7**, 3617–3627.

22 C. He and J. M. Shreeve, *Angew. Chem., Int. Ed.*, 2016, **55**, 772–775.

23 S. Dharavath, J. Zhang, G. H. Imler, D. A. Parrish and J. M. Shreeve, *J. Mater. Chem. A*, 2017, **5**, 4785–4790.

24 O. S. Bushuyev, P. Brown, A. Maiti, R. H. Gee, G. R. Peterson, B. L. Weeks and L. J. Hope-Weeks, *J. Am. Chem. Soc.*, 2012, **134**, 1422–1425.

25 Y. Xu, Q. Wang, C. Shen, Q. Lin, P. Wang and M. Lu, *Nature*, 2017, **549**, 78–81.

26 K. A. McDonald, J. C. Bennion, A. K. Leone and A. J. Matzger, *Chem. Commun.*, 2016, **52**, 10862–10865.

27 C. Zhang, C. Yang, B. Hu, C. Yu, Z. Zheng and C. Sun, *Angew. Chem., Int. Ed.*, 2017, **56**, 4512–4514.

28 C. Sun, C. Zhang, C. Jiang, C. Yang, Y. Du, Y. Zhao, B. Hu, Z. Zheng and K. O. Christe, *Nat. Commun.*, 2018, **9**, 1269.

29 J. G. Xu, C. Sun, M. J. Zhang, B. W. Liu, X. Z. Li, J. Lu, S. H. Wang, F. K. Zheng and G. C. Guo, *Chem. Mater.*, 2017, **29**, 9725–9733.

30 J. G. Xu, S. H. Wang, M. J. Zhang, C. Sun, Y. Xiao, R. Li, F. K. Zheng, G. C. Guo and J. S. Huang, *ACS Omega*, 2017, **2**, 346–352.

31 J. Zhang and J. M. Shreeve, *Dalton Trans.*, 2016, **45**, 2363–2368.

32 X. Liu, W. Gao, P. Sun, Z. Su, S. Chen, Q. Wei, G. Xie and S. Gao, *Green Chem.*, 2015, **17**, 831–836.

33 S. Wang, Q. Wang, X. Feng, B. Wang and L. Yang, *Adv. Mater.*, 2017, **29**, 1701898–1701914.

34 S. Zhang, Q. Yang, X. Liu, X. Qu, Q. Wei, G. Xie, S. Chen and S. Gao, *Coord. Chem. Rev.*, 2016, **307**, 292–312.

35 O. S. Bushuyev, G. R. Peterson, P. Brown, A. Maiti, R. H. Gee, B. L. Weeks and L. J. Hope-Weeks, *Chem. – Eur. J.*, 2013, **19**, 1706–1711.

36 C. Shen, Y. Liu, Z. Q. Zhu, Y. G. Xu and M. Lu, *Chem. Commun.*, 2017, **53**, 7489–7492.

37 S. Li, Y. Wang, C. Qi, X. Zhao, J. Zhang, S. Zhang and S. Pang, *Angew. Chem., Int. Ed.*, 2013, **52**, 14031–14035.

38 H. Zhang, M. Zhang, P. Lin, V. Malgras, J. Tang, S. M. Alshehri, Y. Yamauchi, S. Du and J. Zhang, *Chem. – Eur. J.*, 2016, **22**, 1141–1145.

39 Q. Zhang and J. M. Shreeve, *Angew. Chem., Int. Ed.*, 2014, **53**, 2540–2542.

40 J. D. Lin, J. G. Xu, F. K. Zheng, G. C. Guo, R. X. Lv, W. C. He, Z. N. Huang and J. F. Liu, *J. Solid State Chem.*, 2018, **265**, 42–49.

41 H. L. Boström, J. A. Hill and A. L. Goodwin, *Phys. Chem. Chem. Phys.*, 2016, **18**, 31881–31894.

42 A. K. Cheetham and C. N. R. Rao, *Science*, 2007, **318**, 58–59.

43 Y. L. Sun, X. B. Han and W. Zhang, *Chem. – Eur. J.*, 2017, 11126–11132.

44 W. J. Xu, Z. Y. Du, W. X. Zhang and X. M. Chen, *CrystEngComm*, 2016, **18**, 7915–7928.

45 Y. M. You, W. Q. Liao, D. Zhao, H. Y. Ye, Y. Zhang, Q. Zhou, X. Niu, J. Wang, P. F. Li and D. W. Fu, *Science*, 2017, **357**, 306–309.

46 M. Xue, H. Zhou, X. Yang, J. Mei, L. Yang, C. Ye, J. Zhang and H. Wang, *Sci. China Mater.*, 2017, **5**, 407–414.

47 L. Sun, *Nat. Chem.*, 2015, **7**, 684–685.

48 H.-Y. Ye, Y.-Y. Tang, P.-F. Li, W.-Q. Liao, J.-X. Gao, X.-N. Hua, H. Cai, P.-P. Shi, Y.-M. You and R.-G. Xiong, *Science*, 2018, **361**, 151–155.

49 W. Li, Z. Wang, F. Deschler, S. Gao, R. H. Friend and A. K. Cheetham, *Nat. Rev. Mater.*, 2017, **2**, 16099.

50 G. Feng, X. Jiang, W. Wei, P. Gong, L. Kang, Z. Li, Y. Li, X. Li, X. Wu and Z. Lin, *Dalton Trans.*, 2015, **45**, 4303–4308.

51 S. L. Chen, W. X. Zhang and X. M. Chen, *The 9th National Conference in Inorganic Chemistry — B Coordination Chemistry, Nanchang*, 2015.

52 S. L. Chen, Z. R. Yang, B. J. Wang, Y. Shang, L. Y. Sun, C. T. He, H. L. Zhou, W. X. Zhang and X. M. Chen, *Sci. China Mater.*, 2018, **61**, 1123–1128.

53 W. X. Zhang, S. L. Chen and X. M. Chen, *China Pat.*, ZL201610665880.3, 2016; W. X. Zhang, S. L. Chen and X. M. Chen, *PCT Pat.*, PCT/CN2017/097136, 2017.